Physics Letters A 384 (2020) 126664

Contents lists available at ScienceDirect

Physics Letters A

www.elsevier.com/locate/pla

Nonlinear edge modes in a honeycomb electrical lattice near the Dirac points

F. Palmero [a,*], L.Q. English [b], J. Cuevas-Maraver [c,d], P.G. Kevrekidis [e,f]

[a] Grupo de Física No Lineal, Departamento de Física Aplicada I, Escuela Técnica Superior de Ingeniería Informática, Universidad de Sevilla, Avda Reina Mercedes s/n, E-41012 Sevilla, Spain
[b] Department of Physics and Astronomy Dickinson College, Carlisle, PA, 17013, USA
[c] Grupo de Física No Lineal, Departamento de Física Aplicada I, Universidad de Sevilla, Escuela Politécnica Superior, C/ Virgen de Africa, 7, 41011-Sevilla, Spain
[d] Instituto de Matemáticas de la Universidad de Sevilla (IMUS), Edificio Celestino Mutis, Avda Reina Mercedes s/n, E-41012 Sevilla, Spain
[e] Department of Mathematics and Statistics, University of Massachusetts, Amherst MA 01003-4515, USA
[f] Mathematical Institute, University of Oxford, Oxford, OX2 6GG, UK

ARTICLE INFO

Article history:
Received 17 February 2020
Received in revised form 26 April 2020
Accepted 8 June 2020
Available online 16 June 2020
Communicated by B. Malomed

Keywords:
Intrinsic localized modes
Discrete breathers
Edge breathers

ABSTRACT

We examine - both experimentally and numerically - a two-dimensional nonlinear driven electrical lattice with honeycomb structure. Drives are considered over a range of frequencies both outside (below and above) and inside the band of linear modes. We identify a number of discrete breathers both existing in the bulk and also (predominantly) ones arising at the domain boundaries, localized either along the armchair or along the zig-zag edges. The types of edge-localized breathers observed and computed emerge in distinct frequency bands near the Dirac-point frequency of the dispersion surface while driving the lattice subharmonically (in a spatially homogeneous manner). These observations/computations can represent a starting point towards the exploration of the interplay of nonlinearity and topology in an experimentally tractable system such as the honeycomb electrical lattice.

1. Introduction

Honeycomb lattices have attracted substantial interest within the physics community in recent years, due to their inherent potential of topological surface phenomena [1]. The interplay of topology and wave dynamics (both at the linear and more recently at the nonlinear level) has had significant impact both in the realm of optics [2] and in that of acoustic/mechanical systems [3,4]. Nonlinearity further adds to the complexity and the wealth of this interplay, especially since in settings such as optics [5–8] and atomic physics [9,10], it emerges spontaneously for large amplitude/density excitations.

In two dimensions (2D) the foremost example of honeycomb material is, of course, graphene [11–13]. One of the most intensely studied macroscopic analogues is photonic graphene, and edge-localized states were soon predicted to exist in such materials [14–17]. Furthermore, the role of nonlinearity in this context is beginning to be examined (see e.g., [14,15]), yet there are still numerous avenues worth exploring in this context relating to the impact of nonlinearity, especially in experimentally tractable settings. In the linear regime, some pioneering experimental results have appeared in the literature in photonic graphene that show the existence of edge-localized states [18,19], and these were even shown to propagate in one direction only, upon breaking the time-reversal symmetry [20]. Yet, we argue that the identification of unprecedented, experimentally controlled settings where nonlinear states (both bulk and edge ones) can be obtained is of value to the efforts towards understanding nonlinear topological structures and how they differ from their more standard, non-topological variants (as well as how such states vary from linear topological ones). In that vein, we propose as a platform worth exploring the setting of honeycomb electrical lattices.

More concretely, in this paper we report on a series of findings of nonlinear waves in a 2D electrical honeycomb lattice. That intrinsic localized modes, also known as *discrete breathers* (DBs) can exist in square lattices of this kind has been shown previously [21]. In fact, such modes are well-known to exist in a wide range of physical settings, summarized, e.g., in a number of reviews [22,23]. Here, however, we focus on the role of the honeycomb geometry and drive the system over a wide range of frequencies both within as well as outside the band of small amplitude excitations. We find both experimentally and numerically that not only can bulk-localized modes be identified in this setting, but also edge-localized modes can be excited with a spatially homogenous, sub-

* Corresponding author.
E-mail address: palmero@us.es (F. Palmero).

https://doi.org/10.1016/j.physleta.2020.126664
0375-9601/

harmonic driver. These DBs bear frequencies around that of the Dirac points. The exact DB frequency depends on the wave amplitude, as expected from a soft nonlinear system, but interestingly also on the type of edge. The relevant zig-zag edge-localized DBs are found to exist within a frequency band that is higher, in terms of frequencies (and non-overlapping) compared to the arm-chair mode band. We complement these results with a numerical stability analysis and find that these discrete breathers do not appear to derive from a continuation of linear modes, but that they come into existence via (saddle-node) bifurcation phenomena. Our findings constitute a first step towards the more systematic examination of stable bulk and edge modes in such honeycomb electrical lattices and we hope will spurt further efforts in this direction.

Our presentation is structured as follows. In section 2 we present the mathematical model associated with the experimental setting of interest, i.e., the honeycomb lattice of LC resonators. The underlying linear modes are identified and their band is obtained for parameters associated within the experimental range in Section 3. Subsequently, in section 4, we present an anthology of experimental and numerical results for similar conditions between the experiment and the numerical computation. The findings are presented for different values of the driver frequency, progressively moving from frequencies below the band to ones above the band of linear states. Finally, we summarize our findings and present our conclusions and some challenges arising towards future work in Section 5.

2. The model

The experimental system investigated in this paper is a honeycomb lattice consisting of unit cells in the form of LC resonators, whose nonlinearity is originated by using a varactor diode instead of the standard capacitor. These nonlinear resonators are coupled together into a two-dimensional lattice via coupling inductors. Such a system was studied in a previous publication [21], where it was found that stable two-dimensional ILMs/discrete breathers could be produced. That study used periodic boundary conditions exclusively, thus eliminating any lattice edges. In the present study, we have used free-end boundary conditions, allowing a pair of both zig-zag and armchair edges. This has permitted us to investigate the dynamical interplay between lattice edges and nonlinear localized states.

More concretely, our use of a varactor diode (NTE 618) introduces a specific (experimentally determined) nonlinear capacitance $C(V)$. We also use inductors of value $L_2 = 330$ μH, and the resulting unit cells are driven by a periodic voltage source $\mathcal{E}(t)$ of frequency f (i.e., the driving is *uniform*) via a resistor $R = 10$ kΩ. Each single unit is coupled to its three neighbors via inductors $L_1 = 680$ μH building a honeycomb lattice.

Using basic circuit theory, the system can be described by the equations [21,24],

$$\frac{di_{n,m}}{d\tau} = \frac{L_2}{L_1}\left(\sum_{j,k} v_{j,k} - K_{n,m} v_{n,m}\right) - v_{n,m} \tag{1}$$

$$\frac{dv_{n,m}}{d\tau} = \frac{1}{c(v_{n,m})}\left[i_{n,m} - i^D(v_{n,m}) - \frac{v_{n,m}}{C_0\omega_0 R_e} + \frac{1}{C_0\omega_0 R}\frac{\mathcal{E}(\Omega\tau)}{V_d}\right],$$

where the sum (j,k) is taken over the nearest neighbors of the (n,m) node and $K_{n,m}$ is the number of neighbors of node (n,m). $K_{n,m}$ is equal to three in an infinite lattice (or finite lattice with periodic boundary conditions), but in a finite lattice with free boundaries it could be either $K_{n,m} = 1$ or $K_{n,m} = 2$ on the edges, depending on the particular lattice node. The varactor can be modeled as a nonlinear resistance in parallel with a nonlinear capacitance. As shown in [24], the nonlinear current $I^D(V)$ is given by

$$I^D(V) = -I_s \exp(-\beta V), \tag{2}$$

where $\beta = 38.8$ V^{-1} and $I_s = 1.25 \times 10^{-14}$ A, and its capacitance $C(V)$ as

$$C(V) = \begin{cases} C_v + C_1(V - V_c) + C_2(V - V_c)^2 & \text{if} \quad V \le V_c, \\ C_0 e^{-\alpha V} & \text{if} \quad V > V_c, \end{cases} \tag{3}$$

where $C_0 = 788$ pF, $\alpha = 0.456$ V^{-1}, $C_v = C_0 \exp(-\alpha V_c)$, $C_1 = -\alpha C_v$, $C_2 = 100$ nF and $V_c = -0.28$ V.

The following dimensionless variables were used in Eq. (1): $\tau = \omega_0 t$, where $\omega_0 = 1/\sqrt{L_2 C_0}$; $\Omega = 2\pi f/\omega_0$ is the dimensionless driving frequency; the dimensionless voltage $v_{n,m} = V_{n,m}/V_d$, with V_d representing the voltage amplitude of the driving; $i_{n,m} = (I_v - I_2)/(C_0\omega_0 V_d)$, where I_v is the full current through the unit cell and I_2 the current through the inductor L_2, both corresponding to cell (n,m) and $i^D = I^D/(C_0\omega_0 V_d)$. A phenomenological dissipation resistor, R_l, was included in the model to better approximate the experimental dynamics and R_e is the equivalent resistance so $1/R_e = 1/R + 1/R_l$. In all cases, the ratio L_2/L_1 characterizes the strength of the effective discreteness of the system (with the uncoupled limit obtained for $L_1 \to \infty$). We should add that this is still only a simplified model of the varactor diodes, and comparison between theoretical and experimental results will not be exact. Yet, it is an important first step in the modeling effort towards understanding this setup.

3. Linear modes

In the linear limit ($c(v) = 1$, $i_d = 0$) the undriven and undamped system reduces to

$$\frac{d^2 v_{n,m}}{d\tau^2} = \frac{L_2}{L_1}\left(\sum_{j,k} v_{j,k} - K_{n,m} v_{n,m}\right) - v_{n,m}. \tag{4}$$

Linear modes can be found as plane-wave solutions. An infinite lattice (with nearest neighbor spacing of 1) can be generated from lattice vectors $\mathbf{e}_\pm = (1/2, \pm\sqrt{3}/2)$ (see e.g. [25]), and the dispersion relation $\omega(\mathbf{k})$, with $\mathbf{k} = (k_x, k_y)$, is given by

$$\omega^2 = \frac{1}{C_0 L_2} + \frac{1}{C_0 L_1}\left[3 \pm \sqrt{3 + 2\cos(\sqrt{3}k_y) + 4\cos(3k_x/2)\cos(\sqrt{3}k_y/2)}\right], \tag{5}$$

which yields a band of frequencies between $f_{\min} = \sqrt{1/(C_0 L_2)}/(2\pi) \approx 312$ kHz and $f_{\max} = \sqrt{1/(C_0 L_2) + 6/(C_0 L_1)}/(2\pi) \approx 617$ kHz. As shown in Fig. 1, the band structure corresponds to a graphene-like surface where six Dirac points exist at a frequency of $\omega_d = \sqrt{3/(C_0 L_1) + 1/(C_0 L_2)}$, or $f_d = \omega_d/2\pi \approx 489.11$ kHz.

In a finite lattice, wave vectors $\mathbf{k}$ are quantized. However, this quantization depends on the boundary conditions and the way the lattice is tiled. Because of this, one must be very cautious with the choice of boundary conditions, the way the honeycomb is generated and the lattice size if the Dirac point is intended to be in the linear mode spectrum. For periodic boundary conditions, an explicit expression of the eigenfrequencies can be attained [25], but, for free ends boundary conditions, one must rely on the numerical solution of Eq. (4) for getting the linear mode spectrum.

In the present study, experimental limitations restrict us to a lattice of 6×6 nodes, distributed as shown in Fig. 2. The boundaries are free, as we are interested in seeking edge-localized breathers, as shown below. With this particular choice, there is

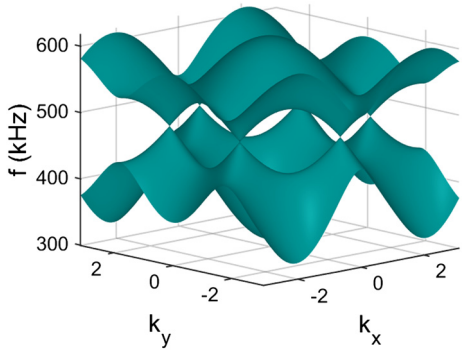

Fig. 1. Typical band structure of the infinite honeycomb lattice in the first Brioullin zone. There are six Dirac points corresponding to $(k_x, k_y) = (0, \pm 4\pi/(3\sqrt{3}))$, $(2\pi/3, \pm 2\pi/(3\sqrt{3}))$, $(-2\pi/3, \pm 2\pi/(3\sqrt{3}))$ and a frequency $f_d = 489.11$ kHz, cf. Eq. (5).

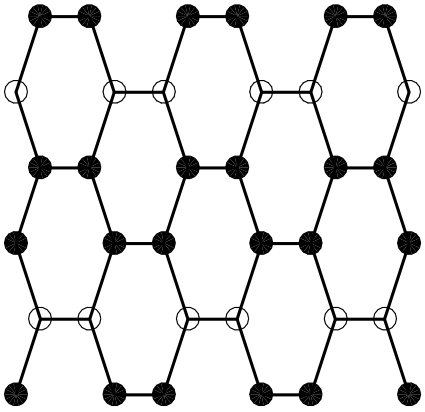

Fig. 2. Finite size (6×6) lattice with free boundaries; shown is the Dirac mode, i.e. the linear mode corresponding to $f = f_D = 489.11$ kHz. Black and white circles correspond, respectively, to a normalized amplitude in $t = 0$ of $1/2$ and -1.

a sole eigenmode oscillating with the Dirac frequency $f = f_d = 489.11$ Hz. Fig. 2 also shows the oscillation pattern of such eigenmode (Dirac mode), which is similar to the oscillation pattern in an infinite lattice. We have checked that this sole Dirac mode is present when tiling this lattice to a larger one with $6N \times 6M$ with $(N, M) \in \mathbb{N}$ nodes.

In addition, the structure of the edges of our lattice can be crucial for the formation of edge-localized breathers. According to the types of edge modes on graphene-like systems [17], our system should be able to support both vertical zigzag and horizontal armchair edge-localized breathers.

4. Nonlinear modes: numerical and experimental results

In this section, we will describe some numerical and experimental results on the existence of DBs when the electric lattice is driven uniformly. We have observed two kinds of such DBs, depending on whether they are localized on the lattice boundaries or elsewhere. We will call these DBs edge breathers (EBs) or bulk breathers (BBs), respectively, hereafter. The latter owe their existence to the intrinsic nonlinearity of the lattice (see e.g. [21,24]). In the former case, there is an interplay between nonlinearity and the nature of the coupling in the vicinity of the boundary. In order to numerically generate nonlinear modes we have to select the right initial conditions but, experimentally, the modes form spontaneously due to noise and instability. I.e., small amplitude excitations are amplified and spontaneously give rise to the formation of the nonlinear coherent waveforms observed. The existence and stability of the breathers depends on the external driving amplitude, its frequency and its shape. In general, upon increasing of external amplitude, breathers have larger amplitude and are narrower, yet at the same time their existence interval is found to shrink. A more detailed study of the range of existence and stability of breathers as a function of amplitude and frequency is out of the scope of this work and could be the focus of further study.

4.1. Driving near the lowest frequency mode

Having constructed the 6×6 honeycomb lattice of Fig. 2, the simplest experiment we can perform is to drive the lattice with a sinusoidal-wave profile and a frequency close the bottom of the linear modes band, as the lowest frequency mode is uniform ($\mathbf{k} = 0$, i.e., the same wavevector as that of the driver). This is performed in a progression of frequencies starting from outside (under) the linear mode band and systematically increasing the frequency of the drive. When the driver frequency is near the bottom of the linear band (i.e. $f \lesssim f_{\min}$), we can generate experimentally both BBs and EBs, where the latter seems to be the most robust state between the two. Under the same conditions, in our theoretical model we find that only EBs exist. Alternatively, the use of periodic boundary conditions enables the existence of BBs for such frequencies. Fig. 3 shows a numerical bulk breather corresponding to a 6×6 lattice with periodic boundaries and its Floquet multipliers spectrum (see e.g. [23] for more details on Floquet analysis for discrete breathers). Recall that the existence of the corresponding multipliers solely within the unit circle for our driven/damped system indicates its spectral stability. In that figure, we also show the experimental BB obtained in the finite size lattice with free boundary conditions. In both cases the driver amplitude was set to 2.1 V and the frequency was 278 kHz. This is a representative example of such BBs within their relevant interval of existence (see also the discussion below).

Similarly, we can induce EBs which are, as indicated above, more robust than BBs. Fig. 4 shows an example of the theoretical and experimental features of an EB whose driving parameters are the same as for the BB of Fig. 3. The existence of both kinds of solutions for the same system parameters indicates the multistability of the system, given the different branches (bulk vs. edge) of solutions. That is, the regions of existence for the different kinds of breathers substantially overlap. The EBs are found to be somewhat more stable in the following sense: as we lower either the frequency or the amplitude of the driver (starting from 278 kHz and 2.1 V), the BB will disappear first, before the EB ceases to exist. This means that there is a small window in driving parameters where only edge breathers can be stabilized. This finding, i.e. the wider range of stabilization of the EB relative to the BB, has been also experimentally observed in a chain of coupled pendula [26].

It should be mentioned that breathers can also be generated via subharmonic driving. In that case, breathers (which are also denoted as *subharmonic breathers*) are characterized by a core (i.e. the peak and large amplitude nodes around it) oscillating with half of the driver frequency whereas tails oscillate with the driving frequency (see [28]). Unlike what is observed in the experiments (featuring both BBs and EBs), it seems that numerically only subharmonic EBs are stable for this 6×6 lattice with free boundaries (the analysis of subharmonic breathers in larger lattices will be the subject of further studies). The observation of long-lived subharmonic BBs in the experiment may be due to small spatial inhomogeneities in the lattice facilitating their stabilization [24]. In terms of the subharmonic EBs, a good agreement is found regarding both their existence and their dynamical robustness.

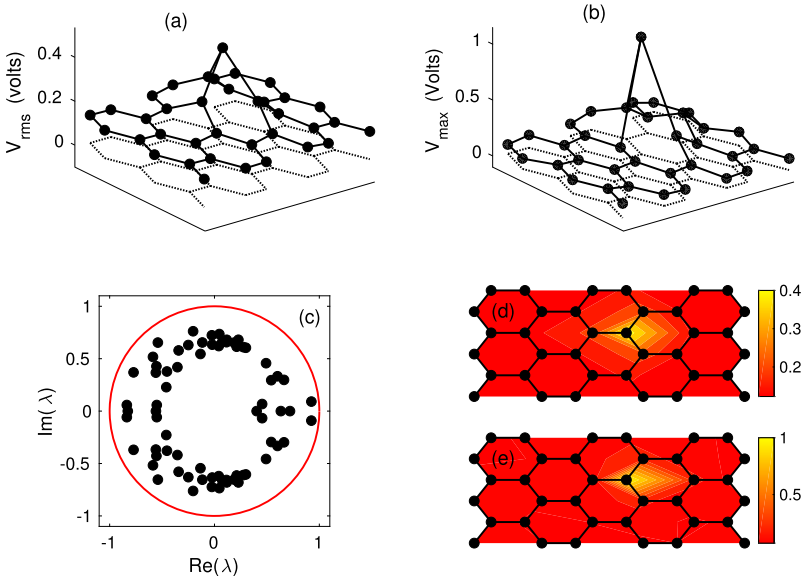

Fig. 3. (a) Numerical bulk breather (BB) profile in a 6×6 lattice with periodic boundaries. (b) Experimental BB in the 6×6 lattice with free boundary conditions. (c) Floquet multiplier spectrum corresponding to the numerical breather showing all the multipliers lying within the unit circle (and thus leading to the conclusion of spectral stability of such breathers). (d, e) Density plots corresponding to (a, b). V_{rms} in panels (a) and (b) stands for the root mean square of the voltage during a period. In both cases the sinusoidal driver amplitude was set to 2.1 V and the frequency was 278 kHz. (For interpretation of the colors in the figure(s), the reader is referred to the web version of this article.)

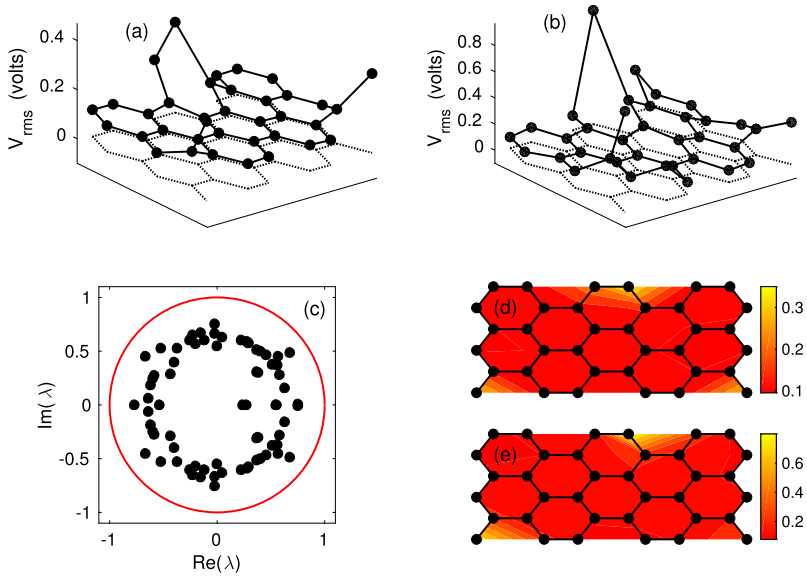

Fig. 4. Same as Fig. 3 but for an edge breather (EB) in a free-boundary lattice.

4.2. *Driving near the Dirac point*

As the driver frequency is increased from around 280 kHz, we first start producing more breathers in the lattice, as expected from previous studies [27]. Then, at higher frequencies, the lattice response gradually weakens. The modes at the Dirac point (with frequency 489.11 kHz) cannot be stimulated directly; this is a consequence of the fact that the Dirac mode possesses a non-zero wavevector, whereas the driver is associated with the zero wavevector.

At higher driving amplitudes, however, lattice response in the vicinity of the Dirac point can be induced via subharmonic driving. Both subharmonic BBs and EBs, which are excited close to the Dirac point frequency, are similar to the ones produced via direct driving although the oscillation frequency of the excited sites is the half of that of the driver and the breather tail (see also Ref. [28]). If the (sinusoidal) driver amplitude is increased to 9 V, a clear lattice subharmonic response is observed in the range $(530, 695)$ kHz. When using a square-wave driving profile, this range is slightly expanded; this phenomenon, which has been reported recently for non-sinusoidal drivings, is related to the enhancement of the "mechanical" impulse transmitted to the lattice from the driver, facilitating the generation of stationary breathers in experiments, as well as in numerical computations [29].

Above the upper edge of this frequency window, the lattice response goes to zero again (at least for the uniform driving used experimentally). Then, starting at 886 kHz and using a square-wave driving at 9 V (no subharmonic response has been found for this range of frequencies using sinusoidal driving), an EB appears firstly along the armchair edge of the honeycomb lattice (also dubbed as

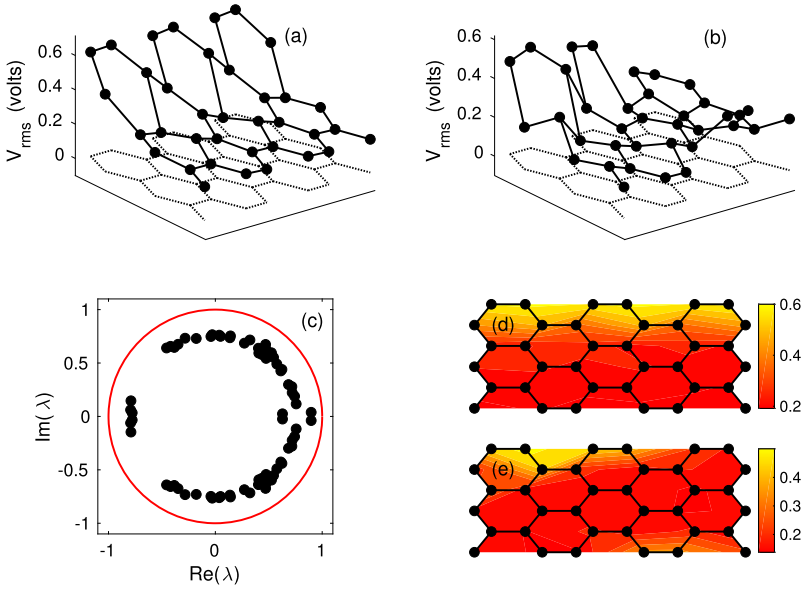

Fig. 5. Same as Fig. 4 but for a subharmonic armchair-EB with a square-wave driving profile of amplitude 9 V. The driving frequency was 960 kHz in numerics and 940 kHz in experiments.

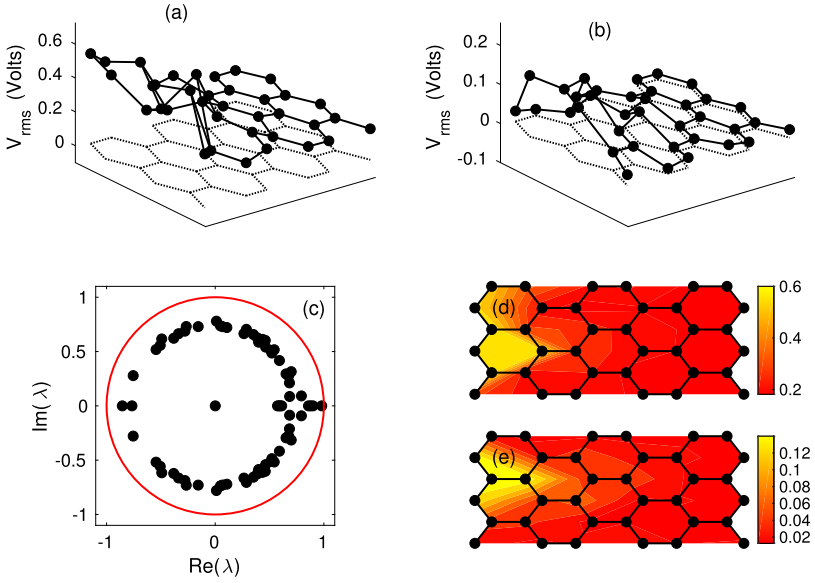

Fig. 6. Same as Fig. 5 but for a subharmonic zig-zag-EB. The driving frequency was 1000 kHz in numerics and 960 kHz in experiments.

armchair-EB). In experiments this mode persists up to a frequency of 940 kHz, corresponding to a response frequency at the breather peak of 470 kHz. Numerical simulations show similar results, as represented in Fig. 5.

At a driver frequency of 950 kHz, we witness an abrupt switch to an EB along the zig-zag edge of the lattice (also dubbed as zig-zag-EB). Such a breather, whose main features are shown in Fig. 6, persists up to a driving frequency of 967 kHz. In general, numerics are in qualitative agreement with the experiments. The switch between these two types of edge breathers as the frequency is adiabatically increased is very reproducible. This clearly suggests the different intervals of stability of the two edge configurations, indicating which one is the system's lower energy state for the different frequency regimes.

Fig. 7 examines the armchair-EB more closely. Here we showcase the most nonlinear, and therefore most localized version of that mode at a driving frequency of 886 kHz. As it can be seen from the experimental pattern depicted in panel (b), there are two of such EBs at the opposite sides of the lattice. Comparing to Fig. 2, one can observe in both cases a sharp localization of the energy at the outermost node-pairs along the armchair edges. It is evident, from the detailed time-dependent oscillations pattern of panel (c), that the two largest-amplitude nodes in the top of the lattice oscillate in anti-phase, indicating that $\mathbf{k} \neq \mathbf{0}$ for this EB. Once again, numerical simulations are in good agreement with experimental results. Similar features (not shown here) are shared with zig-zag-EBs.

In general, the frequency of the main peak of all subharmonic nonlinear modes belongs to the linear spectrum of the infinite lattice. There are multiple features that can allow for this. While the damping changes the spatial extent of the linear modes and the nature of their resonance of breathers with phonons, arguably a

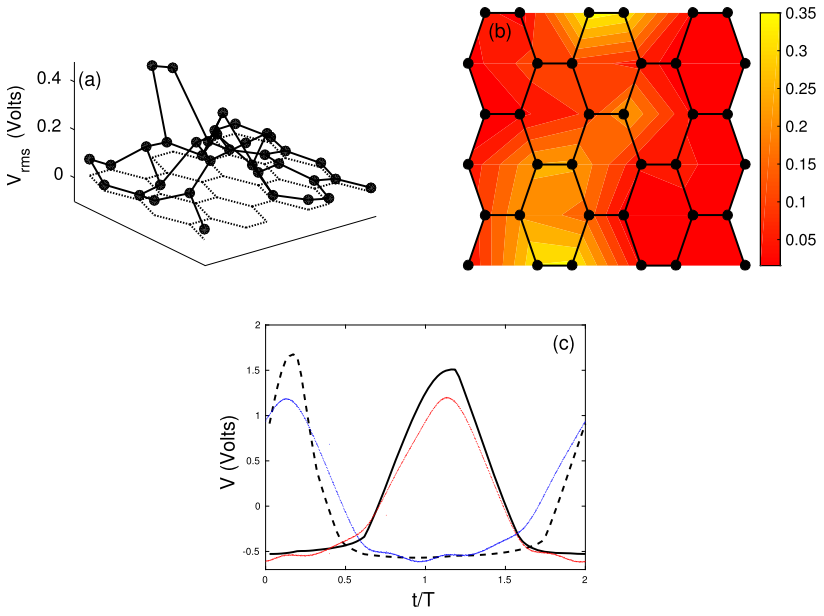

Fig. 7. (a) Experimental subharmonic armchair-EB profile in a 6×6 lattice with free boundaries and (b) its corresponding density plot. The square-wave driving amplitude was set to 9 V and the frequency to 886 kHz. (c) Time dependence of the voltage at the two largest amplitude nodes on the top of the lattice: numerical simulations are shown by black continuous and dashed lines, whereas experimental data are shown in blue and red lines.

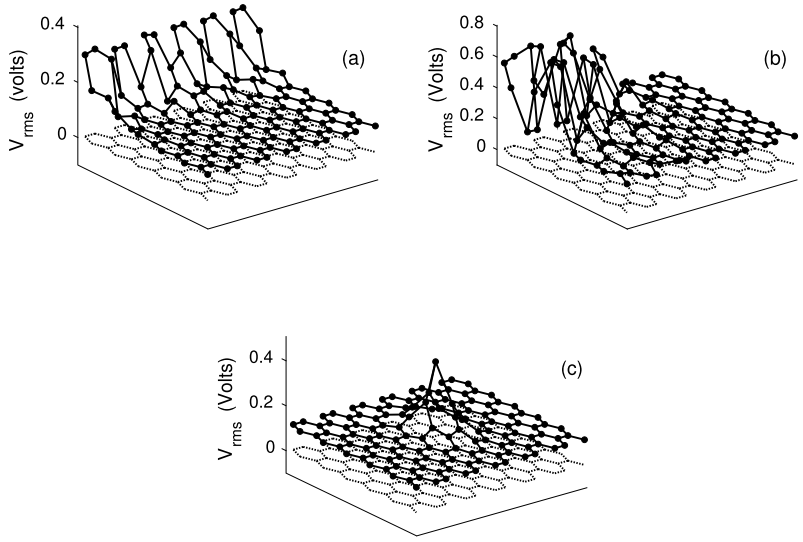

Fig. 8. (a) Same as Fig. 5(a) and (b) Fig. 7(a) in a 12×12 lattice. (c) Numerical bulk breather profile in a 12×12 lattice with free boundaries, where the sinusoidal driver amplitude was set to 2 V and the frequency was 270 kHz.

more central reason is that the small size of the lattices opens gaps in the spectrum allowing for the existence of breathers whose frequency is in one such gap [21,24,28,30].

On the other hand, in order to better understand the nature of edge localization, we have explored the behavior of these localized edge modes in larger lattices. Performing some prototypical numerical computations in a 12×12 lattice, as shown in Fig. 8(a) and (b), the results are qualitatively similar to those obtained in smaller lattices. Note that in order to keep the structure of the phonon band and for the Dirac point to appear, we need to tile the "unit cell" of 6×6 lattice sites. The findings suggest that edge breathers arise as a result of the interplay between the nonlinearity and the finite size of the lattice. Also, numerical bulk breathers exist in free boundary lattices, as shown in Fig. 8 (c).

Edge breathers around the above mentioned frequency ranges i.e. $f \in [886 - 967]$ kHz were not found to occur in the square lattice, thus seeming to be particular to the honeycomb geometry and its associated boundary geometry. Furthermore, it is an interesting fact that zig-zag-EBs and armchair-EBs are found to occupy such distinct frequency bands around the calculated Dirac frequency, as shown in Fig. 9. We do not get any BB with this set of boundary conditions; rather, only EBs arise. An example of a bifurcation diagram featuring a pair of saddle-node bifurcations for numerically calculated subharmonic EBs is shown in Fig. 10. In general, we have found that this scenario of saddle-node bifurcations for the destabilization of solutions is fairly generic (results not shown here) and suggests that breathers may exist in intervals of this sort (amplitude and frequency of the driving). It is only within these intervals, possibly determined via resonance with linear modes, that breathers are found to exist and potentially (as is, e.g., the case for the node branch) be stable. Analyzing such features in more detail turns out to be a rather delicate task due to the existence of nu-

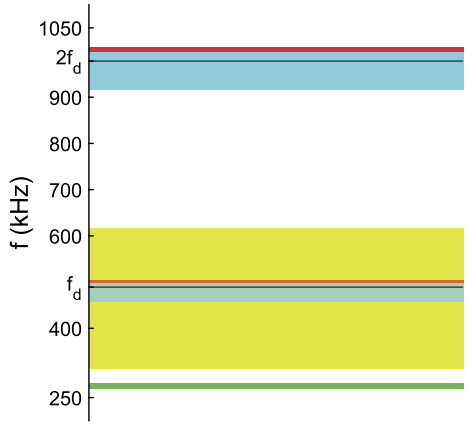

Fig. 9. Stability range versus driving frequency for different kinds of numerically calculated EBs together with the linear modes band, which is represented as a yellow region; Dirac point (f_d) and twice its value are depicted as black horizontal lines. Green region corresponds to (direct-driven) EBs with $V_d = 2.1$ V (cf. Fig. 4). (b) Subharmonic armchair-EBs driven by $V_d = 9$ V (cf. Fig. 5) are represented by the cyan region, and the lighter cyan region overlapping part of the linear modes band corresponds to the subharmonic oscillations of the breather peak. Similarly to the armchair-EB case, the red region and the lighter red one in the linear modes band correspond to subharmonic zig-zag-EBs.

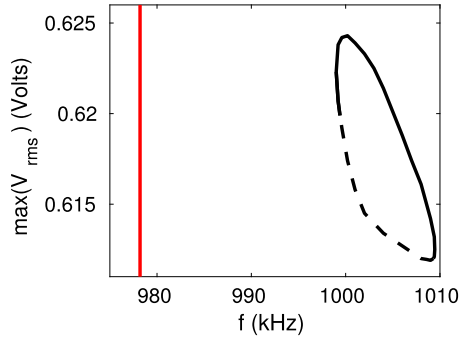

Fig. 10. V_{rms} on peak node of the numerically calculated subharmonic EBs (solutions in red and cyan at Fig. 9), as a function of the frequency. Stable solutions are depicted as continuous lines and unstable solutions as dotted lines. The red line marks twice Dirac frequency ($2f_d$).

merous branches in a complex bifurcation diagram. For this reason, a more exhaustive study is deferred to a future publication.

5. Conclusions & future work

Naturally, the above findings constitute only a first step in the emerging rich study of localized modes and the breathing dynamics in honeycomb electrical lattices. Here, we have explored the arguably most canonical and experimentally more straightforwardly tractable case of a uniform drive of zero wavevector. At frequencies below the linear band, we have found that this drive leads to the formation of bulk, as well as edge breathers, with the latter being more robust than the former. However, our most significant finding concerns the subharmonic drive in the vicinity of twice the frequency of the Dirac point. There, depending on the frequency interval, both armchair and zigzag edge breathers can arise, with each one appearing as the stable state in a respective interval frame.

There are numerous questions that still remain worthwhile to answer. Is it possible to achieve more elaborate forms of driving so as to excite higher order states? At the same time, it appears to be relevant to develop a systematic continuation analysis, e.g., at the Hamiltonian level of the corresponding linear and also subharmonic waves and their expected role in the bifurcation diagram. Understanding whether these edge states enjoy topologically induced propagation properties (e.g. through the lattice boundary) is an important question worth considering in its own right. Furthermore, the experimental tractability of electrical lattices renders them interesting candidates for formulating additional lattices with intriguing topological properties such as, e.g., some of the artificial flat band systems recently summarized in [31].

Declaration of competing interest

The authors declare that they have no known competing financial interests or personal relationships that could have appeared to influence the work reported in this paper.

Acknowledgements

This material is based upon work supported by the US National Science Foundation under Grants No. PHY-1602994 and DMS-1809074 (PGK). PGK also acknowledges support from the Leverhulme Trust via a Visiting Fellowship and the Mathematical Institute of the University of Oxford for its hospitality during part of this work. J.C.-M. was supported by MAT2016-79866-R project (AEI/FEDER, UE) and by project P18-RT-3480 (Regional Government of Andalusia). FP visited Dickinson College with support from the VI Plan Propio of the University of Seville (VI PPITUS). FP also acknowledges Dickinson for its hospitality.

References

[1] B. Andrei Bernevig, Topological Insulators and Topological Superconductors, Princeton University Press, 2013.
[2] L. Lu, J.D. Joannopoulos, M. Soljačić, Nat. Photonics 8 (2014) 821.
[3] R. Süsstrunk, S.D. Huber, Proc. Natl. Acad. Sci. USA 113 (2016) E4767.
[4] G. Ma, M. Xiao, C.T. Chan, Nat. Rev. Phys. 1 (2019) 281.
[5] X. Huang, Y. Lai, Z.H. Hang, H. Zheng, C.T. Chan, Nat. Mater. 10 (2011) 582–586.
[6] O. Peleg, et al., Phys. Rev. Lett. 98 (2007) 103901.
[7] M.J. Ablowitz, S.D. Nixon, Yi Zhu, Phys. Rev. A 79 (2009) 053830.
[8] M.J. Ablowitz, Y. Zhu, Phys. Rev. A 82 (2010) 013840.
[9] L.H. Haddad, L.D. Carr, Physica D 238 (2009) 1413.
[10] L.H. Haddad, L.D. Carr, New J. Phys. 17 (2015) 093037.
[11] K.S. Novoselov, et al., Science 306 (2004) 666; Nature 438 (2005) 197.
[12] A.H.C. Neto, F. Guinea, N.M.R. Peres, K.S. Novoselov, A.K. Geim, Rev. Mod. Phys. 81 (2009) 109.
[13] C. Beenakker, Rev. Mod. Phys. 80 (2008) 1337.
[14] A.V. Savin, Yu.S. Kivshar, Phys. Rev. B 81 (2010) 165418.
[15] A.V. Savin, Yu.S. Kivshar, Europhys. Lett. 89 (2010) 46001.
[16] M.J. Ablowitz, Y.-P. Ma, Opt. Lett. 40 (2015) 4635.
[17] M. Kohmoto, Y. Hasegawa, Phys. Rev. B 76 (2007) 205402.
[18] Y. Plotnik, et al., Nat. Mater. 13 (2014) 57.
[19] J. Noh, S. Huang, K.P. Chen, M.C. Rechtsman, Phys. Rev. Lett. 120 (2018) 063902.
[20] M.C. Rechtsman, et al., Nature 496 (2013) 196–200.
[21] L.Q. English, F. Palmero, J.F. Stormes, J. Cuevas, R. Carretero-González, P.G. Kevrekidis, Phys. Rev. E 88 (2013) 022912.
[22] S. Flach, A.V. Gorbach, Phys. Rep. 467 (2008) 1.
[23] S. Aubry, Physica D 103 (1997) 201.
[24] F. Palmero, L.Q. English, J. Cuevas, R. Carretero-González, P.G. Kevrekidis, Phys. Rev. E 84 (2011) 026605.
[25] J. Cserti, G. Tichy, Eur. J. Phys. 25 (2004) 723.
[26] F. Palmero, J. Han, L.Q. English, T.J. Alexander, P.G. Kevrekidis, Phys. Lett. A 380 (2015) 402.
[27] L.Q. English, R. Basu Thakur, R. Stearrett, Phys. Rev. E 77 (2008) 066601.
[28] L.Q. English, F. Palmero, P. Candiani, J. Cuevas, R. Carretero-González, P.G. Kevrekidis, A.J. Sievers, Phys. Rev. Lett. 108 (2012) 084101.
[29] F. Palmero, J. Cuevas-Maraver, L.Q. English, W. Li, R. Chacón, Phys. Scr. 94 (2019) 065210.
[30] L. Marìn, F. Falo, P.J. Martínez, L.M. Floría, Phys. Rev. E 63 (2001) 066603.
[31] D. Leykam, A. Andreanov, S. Flach, Adv. Phys. 3 (2018) 1473052.